Three-Dimensional Turbulent Flow Code Calculations of Hot Gas Ingestion

Thomas J. VanOverbeke* and James D. Holdeman†
NASA Lewis Research Center, Cleveland, Ohio

The development of short takeoff, vertical landing (STOVL) aircraft has historically been an "experience-based" endeavor. In this study, a three-dimensional turbulent flow computational fluid dynamics (CFD) code was used to calculate the hot gas environment around a STOVL aircraft operating in ground proximity. Preliminary calculations are reported herein for a typical STOVL aircraft configuration to identify key features of the flowfield and to demonstrate the capability of a current three-dimensional CFD code to calculate the temperature of the gases ingested at the engine inlet for typical flow and geometric conditions.

Nomenclature

D_j = side of square lift jets, 0.1133 ft
H = height of lift-jet exhaust above ground plane
T_m = ambient temperature, 70°F
T_j = exhaust-jet temperature, 1000°F
U_m = headwind velocity, 17.8 or 53.7 kt
V_j = exhaust-jet velocity, 1000 ft/s
x = axial coordinate, zero at upstream boundary of calculation domain
x-y = vertical plane aligned in axial direction
x-z = horizontal plane
y = vertical coordinate, zero at ground plane
y-z = vertical plane aligned in transverse direction
z = lateral coordinate, zero at aircraft centerplane

Introduction

SEVERAL concepts for aircraft capable of vertical takeoff and landing have been examined over the past three decades. During this time there have been few successful aircraft of this type. The most notable success, the Harrier,[1] is a subsonic aircraft. There is now a renewed interest in adding short takeoff, vertical landing (STOVL) capability to supersonic fighter aircraft to permit them to return to a short or damaged landing field. To satisfy this requirement, researchers are now examining candidate propulsion system concepts for aircraft with supersonic-cruise and STOVL capability.[2-4] Several of these advanced concepts have proposed increasing lift-jet pressures and temperatures to provide the thrust levels that STOVL aircraft will require. However, these changes would also increase the susceptibility of the aircraft engines to ingestion of hot exhaust gases and, consequently, increase the loss of thrust during flight operations near the ground.

The evaluation of concepts and development of aircraft capable of vertical takeoff and landing has historically been an experience-based endeavor. Several studies of various STOVL aircraft configurations and constituent flows have been published over the past two decades.[5,6] However, three-dimensional computational fluid dynamics (CFD) computer codes are now available that are capable of calculating complex turbulent flows (e.g., Ref. 7). These codes can provide insight into the physics of both internal and external flows, identify the key flow and geometric parameters, and predict flowfield variations resulting from changes in these parameters.

The purpose of the present study was to demonstrate that a publicly available, three-dimensional turbulent-flow CFD code could analyze the hot gas environment around a computer model of a STOVL aircraft in ground proximity. The remainder of this article describes the flow analysis.

Description of the Flowfield and Calculation Domain

In flight operations near the ground, STOVL aircraft typically have a low forward speed and a large fraction of the lift is provided by vectored exhaust or by lift jets. A schematic of the flowfield around this type of aircraft hovering near the ground is shown in Fig. 1.

Because there is evidence of unsteady phenomena in these flowfields, time-accurate experiments and calculations would be preferred. However, these tools are not generally available in a form applicable to complex three-dimensional fluid dynamic problems such as STOVL aircraft in ground effect, and most experimental studies in the literature and in progress (e.g., Ref. 8) are steady-state tests.

In this study, calculations were performed with a three-dimensional, subsonic, TEACH-type turbulent viscous flow code, which solves the time-averaged continuity, momentum, and energy equations in a Cartesian coordinate system by using a hybrid differencing scheme.[9] The momentum and continuity equations are linked by the SIMPLE algorithm.[10] The k-ϵ turbulence model was used to provide closure.

A boxlike shape was specified for the STOVL aircraft fuselage, which was a four-jet, side inlet configuration. The domain of the calculation is shown in Fig. 2. Because the flowfield is symmetric about the aircraft centerplane, only half of the flowfield was calculated. The domain of the calculations was 4.5 ft high, 7.5 ft wide, and 19 ft long. The half-width of the model fuselage was 0.2732 ft, and the sides of the square vertical lift nozzles (D_j) were 0.1133 ft. The distance between the upstream inlet boundary and the engine inlet was 70.6 D_j. The engine inlet was 10 D_j upstream from the centerlines of the forward nozzles. The axial distance between the centerlines of the forward and aft jets was six D_j, and the centerlines of the aft jets were 81.1 D_j upstream of the exit boundary. The side-to-side centerline separation for both forward and aft jets was 3.25 D_j. The width of the engine inlet duct was equal to that of the jets, and its height was about 2.5 D_j.

Presented as Paper 88-2882 at the AIAA 24th Joint Propulsion Conference, Boston, MA, July 11-13, 1988; received July 21, 1988; revision received April 30, 1989.

*Aerospace Engineer, Internal Fluid Mechanics Division.
†Senior Research Engineer, Internal Fluid Mechanics Division. Member AIAA.

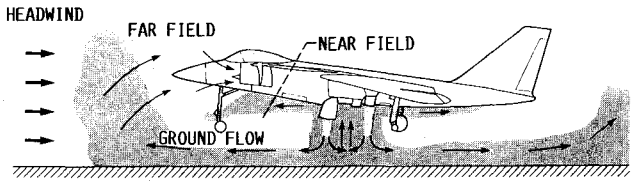

Fig. 1 Flowfield around a STOVL aircraft in ground proximity.

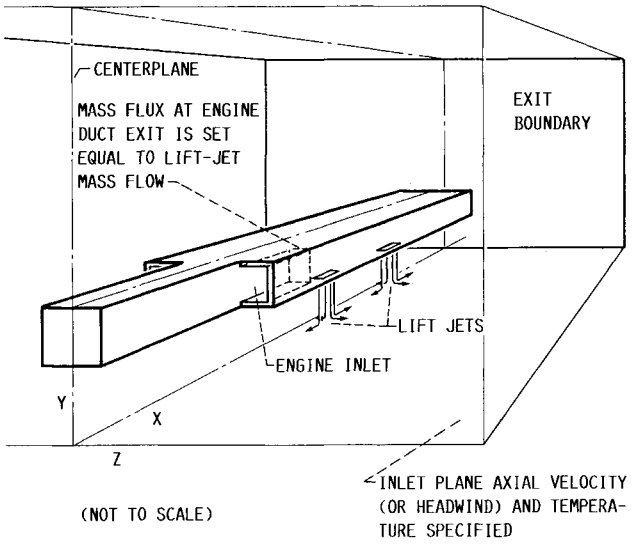

Fig. 2 Computational domain; mass flow at the exit of the engine inlet duct was set equal to that from the lift jets.

The preliminary calculations shown here used 80 axial or x-grid points, 47 y-grid points, and 34 z-grid points. 16 grid cells were used for each nozzle. There were typically 12 x-z planes from the ground plane to the base of the fuselage, and another 12 x-z planes across the height of engine inlet. The walls of the engine inlet duct and the sides of the exhaust jets were one grid cell thick. There were nine x-y planes from the aircraft centerline to the side of the fuselage. A nonuniform grid was used to concentrate cells in the vicinity of the lift jets. Although 127,840 nodes were used in the calculations presented herein, this was, in retrospect, a coarse grid because large gradients in temperature and velocity were found for some flow and geometric conditions, that have been better resolved with a finer grid. Even though the grid used was coarse, these calculations used most of the capability of the computer system available at the time. A portion of a typical calculation grid is shown in Fig. 3.

Uniform temperature and velocity were specified around the fuselage at the upstream boundary. The freestream temperature was 70°F, and the headwind velocity U_m was either 17.8 or 53.7 kt. A mean velocity of 1000 ft/s and a uniform temperature of 1000°F were specified for the vertical lift jets. The turbulence intensity was equal to 6% of the mean velocity at both the mainstream and jet inflow boundries. The turbulence dissipation rate was specified to be 1×10^7 ft^2/s^3 at the jet boundaries, and 25 and 196 ft^2/s^3 at the upstream boundaries for the 17.8 and 53.7 kt headwind cases, respectively.

The jet exhaust flow condition corresponds to a Mach number of 0.53 (nozzle pressure ratio of 1.21), which was considered to be the upper limit of applicability of the subsonic code because it did not include terms to calculate density corrections caused by rapidly changing pressure. These nozzle conditions were comparable to those for the low-pressure tests performed in Ref. 8.

The fuselage behind the jets extended to the exit of the calculation domain. A VonNeumann boundary condition was imposed at the exit of the engine inlet duct and at the down-

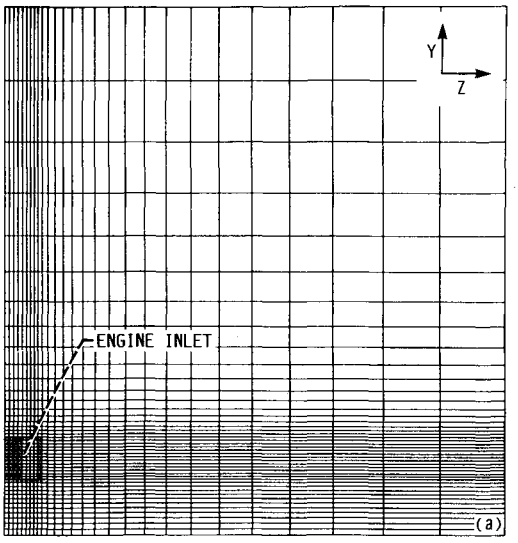

a) Front view

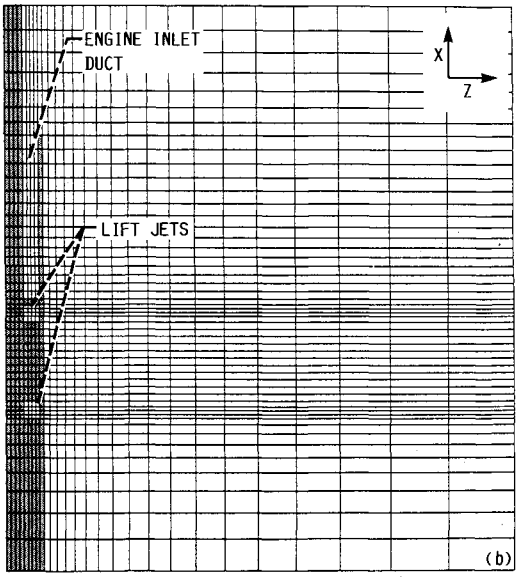

b) Plan view

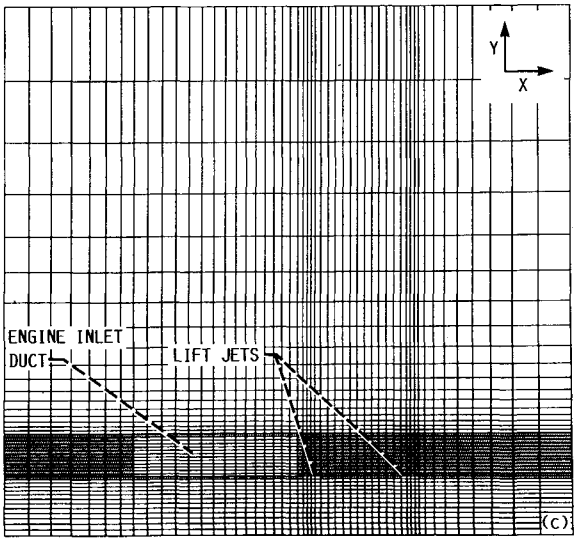

c) Side view

Fig. 3 Portion of a typical 80×47×34 numerical grid

Table 1 Initial and engine inlet conditions for $H/D_j = 4$

Initial conditions[a]		Calculated inlet temperatures, °F		
Headwind velocity U_m, kt	Ratio of headwind to exhaust jet velocity, U_m/V	T_{ave}	T_{max}	T_{min}
17.8	0.03	187.7	388.2	109.8
53.7	0.09	145.1	469.9	61.6

[a]Ambient temperature, 70°F; exhaust-jet temperature, 1000°F; nozzle pressure ratio, 1.21.

stream flowfield exit. A symmetric boundary condition was used along the aircraft centerplane. A no-slip, adiabatic wall boundary condition was imposed at the ground plane on all aircraft surfaces and at the sidewall boundaries of the calculation domain. The computer code was modified to conserve mass between the vertical lift jets and the aircraft engine inlet.

For large calculations, convergence within 5% (total residual divided by some appropriate nondimensionalizing number) is typical. However, because most of the changes in the flowfield in these calculations occur in a very small portion of the calculation domain, these calculations were run to lower values of the residual (e.g., 0.26% for $U_m/V_j = 0.03$, $H/D_j = 4$), with the calculation terminated when the averaged temperature at the exit of the engine inlet duct suggested that the calculation had converged. Typically, 2000 or more iterations were required to satisfy this criteria. Details of the numerical model, the calculation procedures used in this study, and a more comprehensive presentation of the results are given in Ref. 11. The initial velocity and temperature conditions and the corresponding calculated inlet temperatures are given in Table 1.

Results

Features of the calculated hot gas environment are shown for headwind speeds of 17.8 and 53.7 kt ($U_m/V_j = 0.03$ and 0.09), with the base of the aircraft fuselage located at a distance equal to four exhaust-jet diameters above the ground plane ($H/D_j = 4$). For each case, ground-plane velocity and temperature distributions beneath the aircraft are shown, as are selected distributions in vertical planes. The color distribution on these plots varies linearly with temperature.

Color figures are shown for the temperature distributions in preference to the more conventional contour plots, because they show hot and cold regions better than contours, which emphasize gradients rather than temperature levels. Although quantitative information is, of course, available from the calculations, it was not the purpose of the present study to provide quantitative temperature predictions for direct comparison with experiments nor to perform a parametric study of the effects on the flowfield of varying flow and geometry parameters.

Features of the Flowfield

Ingestion of hot gases by the engine inlet may have two adverse effects on aircraft operating in the STOVL flight regime: 1) an average rise in engine inlet temperature may cause a decrease in engine thrust, and 2) a temperature distortion may cause the engine to stall. Engine exhaust gases may be ingested by either far- or near-field mechanisms (see Fig. 1).

In the far-field mechanism, the exhaust gases from the lift jets impinge on the ground plane to form radial wall jets. Forward-flowing sections of the expanding wall jets are slowed by the headwind and, because of their buoyancy, separate from the ground and rise to mix with the ambient air. This fluid can then be drawn back into the engine inlet. The temperature of gases ingested at the engine inlet by this mechanism depends on the aircraft configuration, ground proximity, and flight speed.

Near-field ingestion occurs with multiple jet configurations. In these configurations, an upflow (fountain) is caused when outflowing wall jets from two adjacent lift jets meet. This fountain flow can then impinge on the underside of the fuselage. High inlet temperature levels can occur when these gases are allowed to flow along the fuselage to the vicinity of the engine inlets and are ingested. The gases ingested by this near-field mechanism tend to be hotter, and result in greater tem-

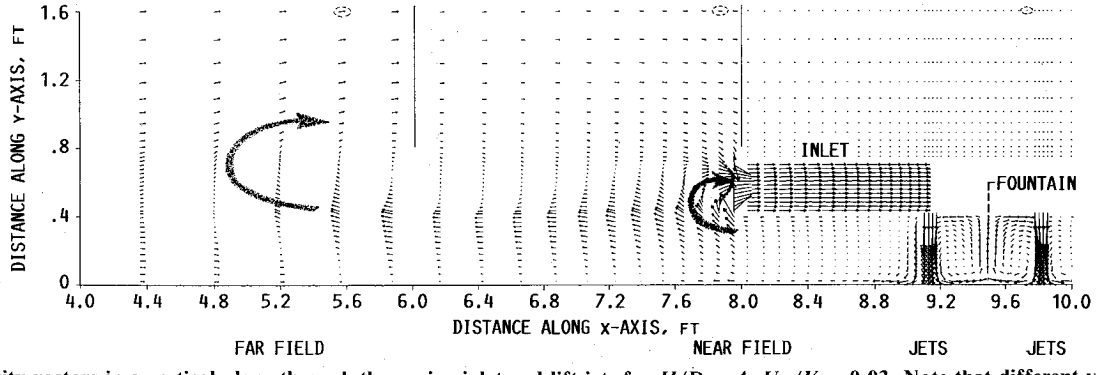

Fig. 4 Velocity vectors in a vertical plane through the engine inlet and lift jets for $H/D_j = 4$, $U_m/V_j = 0.03$. Note that different velocity scales have been used at different axial distances from the lift jets. Circled arrows represent approximately 17.8 kt.

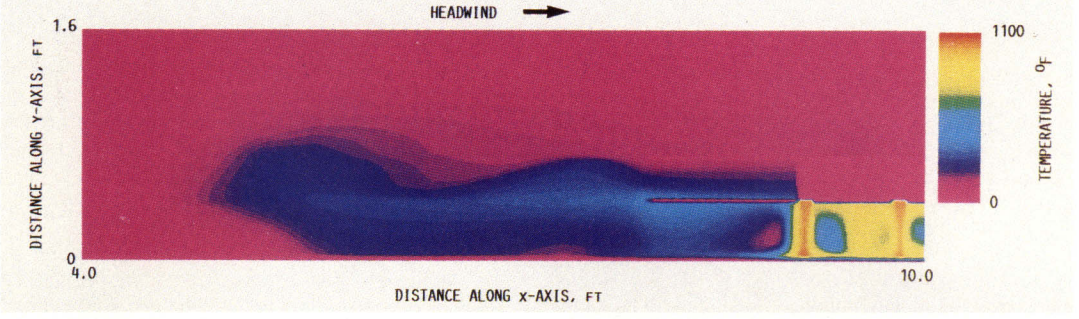

Fig. 5 Smoothed temperature distribution in a vertical plane (x-y) through the engine inlet and lift-jets for $H/D_j = 4$, $U_m/V_j = 0.03$.

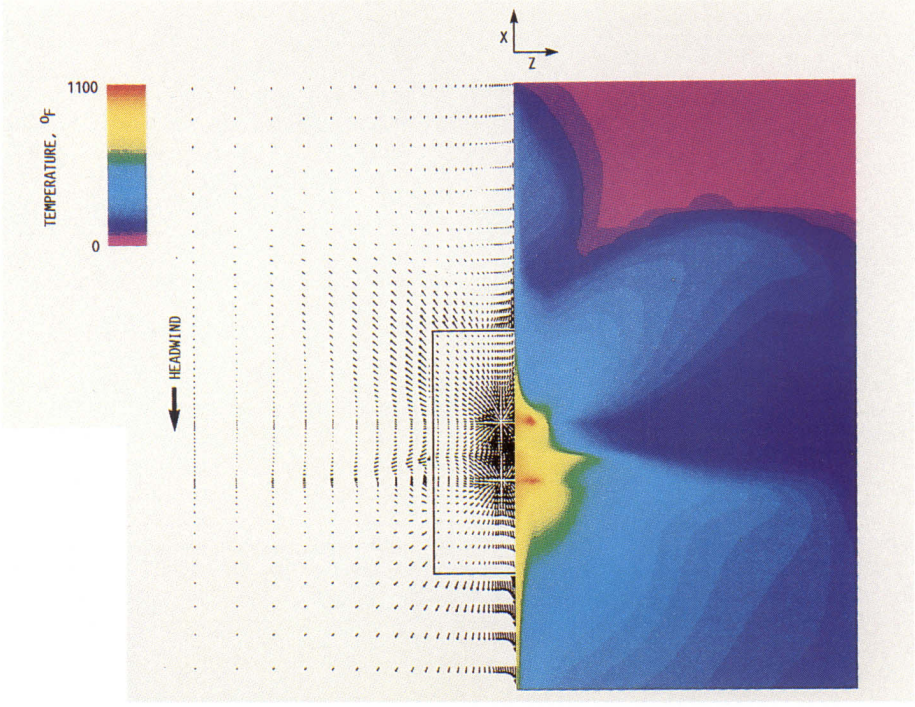

Fig. 6 Smoothed ground-plane (x-z) temperature distribution for $H/D_j = 4$, $U_m/V_j = 0.03$.

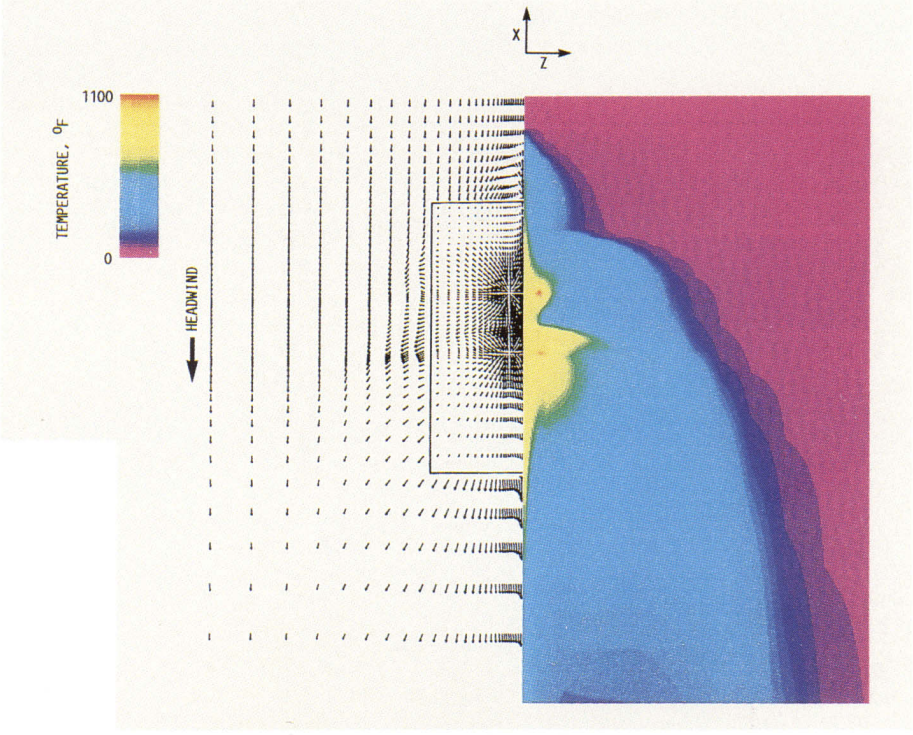

Fig. 7 Smoothed ground-plane (x-z) temperature distribution for $H/D_j = 4$, $U_m/V_j = 0.09$.

perature distortion than those ingested by the far-field mechanism.

These features are shown in the results that follow, where the hot gas environment is shown by calculations for $U_m/V_j = 0.03$ and $H/D_j = 4$. In Fig. 4, near-field and far-field flows are shown in the velocity vectors plot of a vertical plane through the engine inlet and lift jets. In this figure, different velocity scales were used at different axial distances from the lift jets to better show the direction of the flow. These regimes are separated by the light vertical lines in the figure. The encircled velocity vectors in each region represent approximately 17.8 kt. The impingement of the jets on the ground plane and the subsequent redirection of the flow is evident in the figure. The forward extent and overall motion of the far-field flow is indicated by the large arrow and shaded line. Near-field ingestion from along the base of the fuselage is also indicated by a large arrow.

Figure 5 shows the temperature field corresponding to the velocity field in Fig. 4. Note the correspondence between the temperature and velocity fields, in particular the region of warm gas that extends forward of the inlet corresponding to the ground vortex flow.

Variation of Headwind Speed

The effect of variations in the strength of the headwind can be seen by comparing calculated results for $U_m/V_j = 0.03$ and 0.09, with $H/D_j = 4$. Figure 6 shows temperature and velocity distributions in the first x-z plane above the ground for the case with the weaker headwind. In this figure, the aircraft is pointing toward the top of the figure, with the headwind flow from top to bottom.

The location where the jets impinge on the ground plane is evident in Fig. 6. The flow is radially outward from each of these points. Flow components along and perpendicular to the aircraft centerline, midway between the forward and aft jets, are evident in the figure. Note that the outer boundary of the warm region, at about 45 deg to the fuselage centerline (clockwise from the top of the figure), is bent rearward (down) by the headwind.

Figure 7 shows the temperature and velocity fields in an x-z plane near the ground for the same aircraft configuration, but with a stronger headwind ($U_m/V_j = 0.09$). The most obvious effect of the stronger headwind is the downwind sweep of the flow from the aircraft lift jets. Also note that the forward hot gas flow stagnates closer to the engine inlets with the stronger headwind. The side flow between the forward and aft jets that is particularly evident in both Figs. 6 and 7 is consistent with the flow visualization results in Ref. 8.

Temperature distributions in three vertical axial x-y planes are shown in Figs. 8 and 9 for weak and strong headwind flow, respectively. The headwind is from left to right in these figures. Figures 8a and 9a correspond to the aircraft centerplane; Figs. 8b and 9b contain the first x-y plane through the engine inlet, and Figs. 8c and 9c contain the second vertical calculation plane away from the side of the aircraft fuselage.

Along the aircraft centerplane, flow is hottest near the ground. The temperatures are also hotter between the aft lift jets and the upward flow of the fountain than between the fountain and the forward lift jets. Ingestion of hot exhaust gases by the engine inlet is indicated in both cases. With the stronger headwind, the stagnation region is just upstream of the engine inlet and corresponding steep temperature gradients are apparent in this region, with hot gases ingested primarily in the lower section of the inlet.

The calculated dimensionless average inlet temperatures and the temperature distortion of these cases are given in Table 2. The average dimensionless temperature difference ratio is defined as the average inlet temperature rise divided by the difference between the lift-jet temperature 1000°F and the ambient temperature 70°F. The dimensionless inlet temperature distortion is defined as the difference between the maximum and minimum inlet temperatures divided by the difference between the jet and ambient temperatures. For $H/D_j = 4$, the average dimensionless inlet temperature rise decreased from 0.13 to 0.08 when U_m/V_j was increased from 0.03 to 0.09, whereas the maximum dimensionless temperature distortion increased from 0.30 to 0.44 (see Table 2).

Figure 10 shows the temperature distributions in the first y-z plane through the inlet duct for the two cases shown in this

Table 2 Dimensionless engine inlet temperatures for $H/D_j = 4$

Ratio of headwind to exhaust jet velocity, U_m/V_j	Average inlet temperature $(T_{ave}-T_m)$	Inlet temperature distortion $(T_{max}-T_{min})/(T_j-T_m)/(T_j-T_m)$
0.03	0.13	0.30
0.09	0.08	0.44

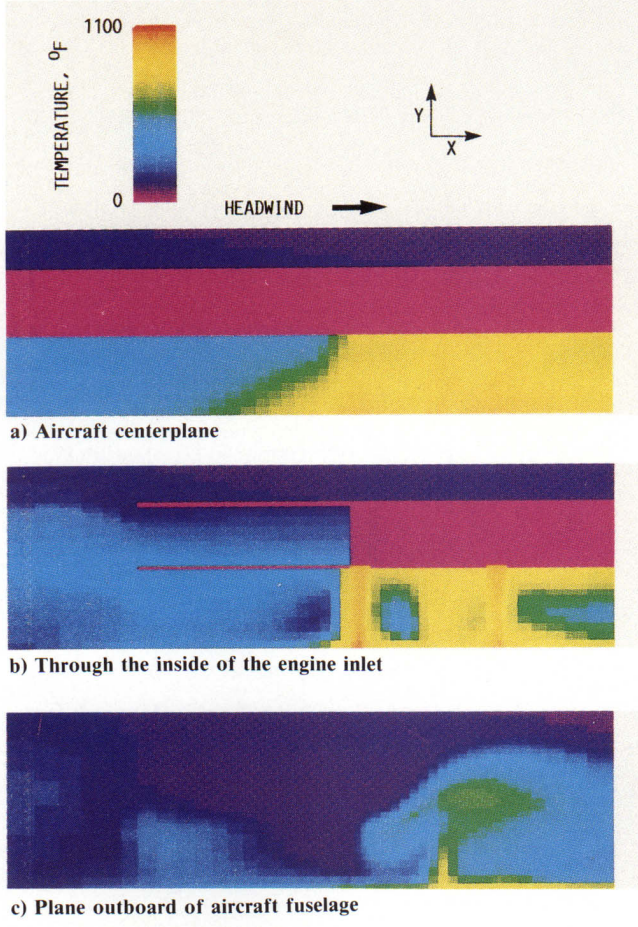

a) Aircraft centerplane

b) Through the inside of the engine inlet

c) Plane outboard of aircraft fuselage

Fig. 8 Temperature distributions in vertical axial (x-y) planes for $H/D_j = 4$, $U_m/V_j = 0.03$).

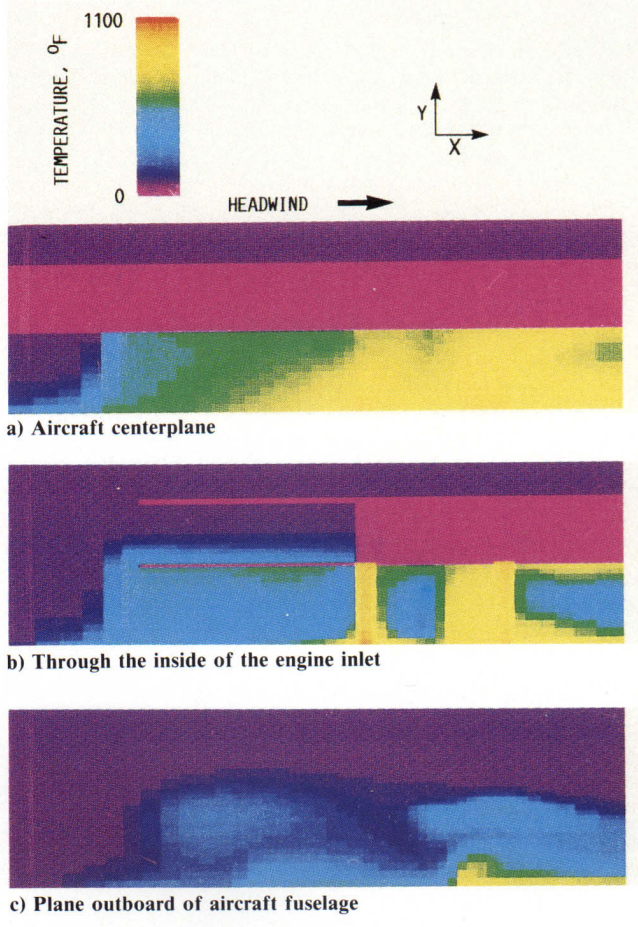

a) Aircraft centerplane

b) Through the inside of the engine inlet

c) Plane outboard of aircraft fuselage

Fig. 9 Temperature distribution in vertical axial (x-y) planes for $H/D_j = 4$, $U_m/V_j = 0.09$).

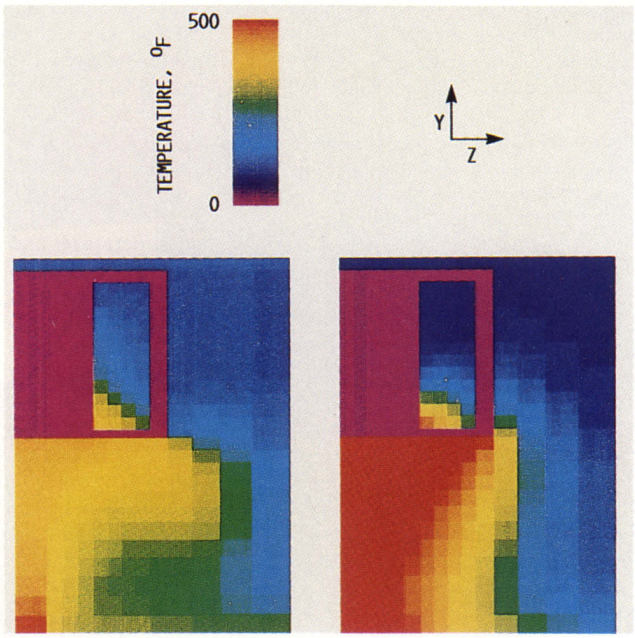

a) $U_m/V_j = 0.03$ b) $U_m/V_j = 0.09$

Fig. 10 Comparison of temperature distributions in the first vertical transverse (y-z) plane through engine inlet for $H/D_j = 4$.

paper. A different temperature scale has been used in Fig. 10 to better show the range and distribution of temperatures in the engine inlet. Temperatures in the inlet duct are highest in the lower inside corner, consistent with the results reported in Ref. 12. The contribution of near- and far-field mechanisms to ingestion depends on the location of the stagnation of the forward-flowing hot gases. Increasing headwind strength will move the stagnation closer to the jets with increasingly steep temperature gradients, so the computational grid may need to be adjusted in that region. These results suggest that temperature distortion would be expected to increase with increasing headwind strength, but note that if the headwind were stronger, so that the stagnation region were downstream of the engine inlet, there would be no ingestion of hot exhaust gases.

Summary of Results

Exhaust gases were ingested in all cases shown here and in Ref. 11. The warmest inlet temperatures were located in the lower inside corner of the engine inlet duct, with greater temperature distortion attributable to near-field ingestion. For the cases with a strong headwind, the hot gas ingestion was mostly from hot gas directed forward along the bottom of the fuselage. Far-field ingestion was particularly evident in the cases with the weaker headwind, and led to warmer average inlet temperatures.

Concluding Remarks

Calculations made with a three-dimensional, turbulent-flow, TEACH-type CFD code in this analysis of the hot gas environment around a STOVL aircraft showed the key features in the flowfield, as identified, for example, in Refs. 5 and 8. Previous studies (e.g., Ref. 7) showed that calculations made with this type of code tended to quantitatively underpredict the mixing. However, Ref. 7 also showed that this type of code was capable of correctly describing the trends shown in experimental data, such that relative comparisons could be made with confidence.

Quantitative accuracy could be improved with advanced turbulence and scalar transport models, less diffusive numerical differencing schemes, and at least twice as many grid-points. The latter two improvements require the use of larger and faster computers. In addition, because many of the propulsion systems now being proposed for advanced STOVL aircraft will use choked or underexpanded exhaust jets, calculation of the hot gas environment around these aircraft will require a code capable of calculating flows that have regions of compressible flow embedded in a large low-speed subsonic flow. Finally, body-fitted coordinates would be needed to model a more realistic aircraft and to examine the effects of angle of attack on the hot gas environment.

References

[1]Sweetman, B., *Harrier*, Jane's, London, England, 1984.

[2]Lewis, W. J., and Palfreyman, D., "Supersonic V/STOL Ready for Technology Push," *Aerospace America,* Vol. 22, Oct. 1984, pp. 46–51.

[3]Holt, D., "Supersonic V/STOL: Will it Happen?" *Aerospace Engineering,* Vol. 7, Nov. 1987, pp. 8–13.

[4]Batterton, P. G., and Blaha, B. J., "NASA Supersonic STOVL Propulsion Technology Program," *International Powered Lift Conference and Exposition,* Society of Automotive Engineers, Warrendale, PA, 1988, pp. 483–494; also, NASA TM-100227.

[5]Kuhn, R. E., "Design Concepts for Minimizing Hot-Gas Ingestion in V/STOL Aircraft," *Journal of Aircraft,* Vol. 19, Oct. 1982, pp. 845–850.

[6]Kuhn, R. E., and Eshleman, J., "Ground Effects on V/STOL and STOL Aircraft—A Survey," AIAA Paper 85-4033, 1985; also, NASA TM-86825.

[7]Mongia, H. C., Reynolds, R. S., and Srinivasan, R., "Multidimensional Gas Trubine Combustion Modeling: Applications and Limitations," *AIAA Journal,* Vol. 24, June 1986, pp. 890–904.

[8]Johns, A. L., Flood, J. D., Strock, T. W., and Amuedo, K. C., "Hot Gas Ingestion Testing of an Advanced STOVL Concept in the NASA Lewis 9′ × 15′ Low Speed Wind Tunnel with Flow Visualization," AIAA Paper 88-3025, July 1988; also, NASA TM-100952.

[9]Syed, S. A., and James, R. H., "User Manual for 3-D-Teach With Rotation," NASA CR-180886, 1988.

[10]Patankar, S. V., *Numerical Heat Transfer and Fluid Flow,* Hemisphere, Washington, DC, 1980.

[11]VanOverbeke, T. J., and Holdeman, J. D., "A Numerical Study of the Hot Gas Environment Around a STOVL Aircraft in Ground Proximity," AIAA Paper 88-2882, July 1988; also, NASA TM-100895.

[12]Gray, L. and Kisielowski, E., "Practical Engineering Methods for Predicting Hot Gas Reingestion Characteristics of V/STOL Aircraft Jet-Lift Engines," NASA CR-111845, 1971.

Color reproduction courtesy of NASA Lewis Research Center